Experiments in Fluids (2022) 63:167
https://doi.org/10.1007/s00348-022-03507-5

RESEARCH ARTICLE

Planar Interferometric Tracking of droplets in evaporating conditions

Hywel Davies[1] · Midhat Talibi[1] · Andrea Ducci[1] · Nishant Parsania[2] · Ramanarayanan Balachandran[1]

Received: 1 April 2022 / Revised: 19 August 2022 / Accepted: 13 September 2022 / Published online: 20 October 2022

Abstract

An effective Lagrangian Planar Interferometric Tracking (PIT) processor is proposed to track the size and path of multiple droplets, with spray droplet diameters (20–150 μm) and volumetric concentrations (≈300 drops/cm^3) consistent with industrial applications, produced by an ultrasonic atomiser in evaporating conditions. A test facility was developed where liquid droplets are exposed to a temperature gradient in a co-axial air flow, where the outer stream is preheated to the desired temperature (288–550 K). The PIT method builds on a TSI Global Sizing Velocimtery measurement technique and allows to detect, size and follow the path of droplets which were otherwise discarded or mis-analysed by the commercial software. The methodology was first tested under non-evaporating conditions, and multiple sources of errors, some common to most planar interferometric techniques, were identified and their order of magnitude and impact on final droplet measurement assessed. The main source of error is related to the out-of-plane motion of the droplets and the time they spend in the measurement volume. For non-evaporating conditions, measured data can be processed to filter out this source of error. In evaporating conditions, a novel method for assessing the impact of measurement error with respect to droplet evaporation and measurement timescales is defined. The PIT method allowed tracking of individual methanol droplets entrained within an airflow heated to 495 K and determining their size reduction under evaporating conditions. Measured droplet evaporation rates were then compared against those predicted by an iterative evaporation model, and a very good agreement was found between the modelled and measured estimates.

Graphical abstract

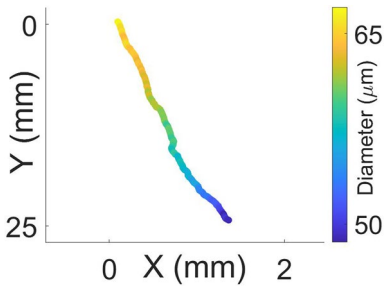

✉ Hywel Davies
hywel.davies.14@ucl.ac.uk

Midhat Talibi
m.talibi@ucl.ac.uk

Andrea Ducci
a.ducci@ucl.ac.uk

Nishant Parsania
nishant.parsania@siemens-energy.com

Ramanarayanan Balachandran
r.balachandran@ucl.ac.uk

[1] Department of Mechanical Engineering, University College London, London WC1E 7JE, UK

[2] Siemens Energy Industrial Turbomachinery Ltd, Lincoln LN5 7FD, UK

1 Introduction

Droplet evaporation plays a crucial role in numerous industries, from pharmaceuticals to energy generation, and reliable, accurate measurements of this physical process are essential to develop empirically derived evaporation models and inform infrastructure design and implementation. For example, such models often define the required temperatures in a spray drying facility (Cotabarren et al. 2018) or provide an estimate of the expected droplet size distribution at the point of ignition in combustion engines (Sazhin 2006). Thus, the importance of having accurate and applicable evaporation models for industry is apparent.

Though much fundamental research has been performed in combustion and spray applications and several empirical evaporation models have been produced to address droplet evaporation in generalised cases (Hubbard et al. 1975) or for specific applications under relevant operating conditions for the vaporisation of fuel sprays (Abramzon and Sirignano 1989), their reliability and applicability to a broader range of scenarios are hindered by the accuracy and limitations of the measurements methods to acquire the data used in the model fitting process and validation.

Typical experimental methods involve the suspension of a single liquid droplet along a fibre, thus creating a stationary droplet that can be repeatedly sized in time through optical measurements (Strizhak et al. 2018). This methodology comes with an obvious limitation as the fibre acts as a conduit for heat conduction to the centre of the liquid droplet, thus affecting the measured evaporation process. To avoid the impact of droplet suspension fibres (Chauveau et al. 2019), acoustic levitation approaches have been developed to fix the position of a droplet in space (Yarin et al. 1999). However, this single-droplet approach to measure evaporation is still subject to several limitations, such as the difficulty to incorporate the effects of droplet volumetric concentration and multi-droplet interactions (Labowsky 1976) and the effects of local and time-dependent flow field variations, such as those present in oscillating flows (Sujith et al. 2000). With regard to fuel spray vaporisation, Sahu et al. (2018) observed that lower droplet evaporation rates are present at higher levels of droplet volumetric concentration. These observations are in agreement with theories developed for combustion of droplet groups outlined by Chiu et al. (1982), whilst Balachandran et al. (2008) noted that the presence of acoustic oscillations enhanced droplet evaporation in a bluff body combustor.

Ideally measurements of the evaporation of free droplets should be carried out for spray conditions consistent with those encountered in industrial applications, thus providing a thorough characterisation of the evaporation process occurring in the actual infrastructure used within a given industry. However, given the complexity of the flow dynamics within "realistic" spray evaporation processes, measurements in such conditions are often simplified to the comparison of time-averaged droplet diameter profiles at two or more locations within the spray. Such an approach does not allow to assess the impact of individual droplet characteristics, such as size and velocity, on the measured evaporation rates.

In order for a measurement method to directly determine evaporation rates of individual droplets, the measurement technique must be able to detect, size and track each droplet in time and space. The process of droplet tracking is not a novel concept with techniques such as Particle Tracking Velocimetry (PTV) having been shown to be effective measurement methods. However, these methods are not capable of providing a measure of droplet diameter and thus are not suitable in these instances. Relatively few techniques can provide a direct measurement of individual droplet size and velocity. These include Phase Doppler Anemometry (PDA), Digital Inline Holography (DIH), high-magnification Particle Tracking Velocimetry (PTV) and Interferometric Droplet Sizing (IDS). Whilst PDA can record the diameter of individual droplets and has been used extensively to measure droplet velocity and diameter (Bachalo and Houser 1984; Sommerfeld 1998), it is inherently a point measurement technique and there is no evident way in which it can be used to make multiple measurements of the same droplet over time to determine the rate of evaporation. IDS techniques, however, operate with a considerably larger measurement volume (Kobayashi et al. 2000), where with the correct imaging frequency and imaging window dimensions for the given flow field velocities, a single droplet can remain in the measurement volume for multiple image captures (Kawaguchi et al. 2010). Both DIH and high-magnification PTV methods have been shown to be capable of effectively tracking and sizing droplets (Guildenbecher et al. 2016; Bautista-Capetillo et al. 2014). However, the lower measurable droplet diameter is limited by optical resolution, determined by the optical setup used (Falgout et al. 2019; Lieber et al. 2019). Thus, when observing the evaporation of smaller droplets within a flow, higher optical magnifications may be required, reducing the imaging field of view and time duration (thus number of diameter measurements) over which droplet evaporation may be measured (Chen and Guildenbecher 2017). IDS techniques, however, require lower optical resolution in order to achieve ideal minimum measurable droplet diameters due to the measurement principles in use.

A number of currently available IDS techniques such as Global Sizing Velocimetry (GSV) from TSI® use a double image system with short inter-capture interval to allow for measurements of droplet velocity along with droplet size (Pan et al. 2006). It stands to reason that this

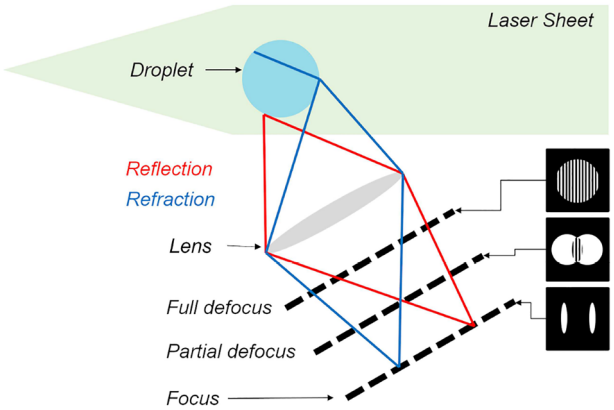

Fig. 1 Diagram showing interaction of reflected and refracted light scattered from a single droplet, at various degrees of camera defocus

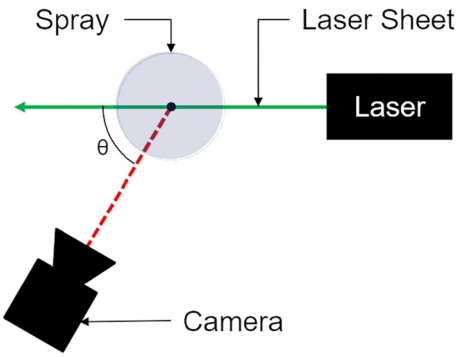

Fig. 2 Top-down view of a typical laser–camera–spray setup seen for IDS experiments

methodology could be expanded across more than two image captures, providing not only the "instantaneous" droplet diameter and velocity, but also the variation in time of droplet velocity (acceleration), droplet trajectory and, pertinent to this study, the rate of change of droplet diameter. Indeed, these aspects have been addressed in a previous study by Kawaguchi et al. (2010). In their work, ethanol droplets were tracked over multiple frames from which the size reduction due to evaporation in a heated jet was measured. The authors then determined the evaporation rate constant and estimated evaporation times, over measurement duration of up to 14 ms, for a very small number of individual droplets. More recently, a similar IDS tracking technique was proposed and implemented by Parant et al. (2021), where the time and position of dodecane droplets entering a methane flame and subject to rapid evaporation were estimated, though the presence of burnt gasses prevented direct measure of individual droplet size reduction over time. Despite the potential benefits of an interferometric tracking system, the literature describing its use, benefits and potential limitations is extremely limited.

In the current study, an in-house Lagrangian Planar Interferometric Tracking (PIT) processor, developed in MATLAB, in conjunction with an existing IDS technique, the Global Sizing Velocimetry (GSV) from TSI®, is applied to a non-evaporating water spray to assess tracking performance and facilitate the observation of measurement uncertainties. The PIT technique is then applied to a methanol spray in a heated coaxial air flow, where droplet evaporation is measured and compared with a modified empirically derived evaporation model.

1.1 Principles of interferometric droplet sizing

Interferometric droplet sizing techniques use both the reflected and refracted images from droplets to accurately determine their diameters. Figure 1 outlines the principles of IDS, displaying the interaction between the reflected and refracted light from a single droplet and the associated interference pattern at progressive degrees of camera defocus. The camera is set at a scattering angle, θ, to the laser plane in order capture both reflected and refracted images, as shown in Fig. 2. The camera is then deliberately defocused, so that the reflected and refracted images superpose, creating an interference pattern. The droplet diameter D is directly estimated from the fringe angular spacing, $\Delta\zeta$ using Eq. 1, where λ is the laser wavelength and X is a constant based upon the scattering angle and liquid refractive index.

$$D = X \cdot \frac{\lambda}{\Delta\zeta} \tag{1}$$

Additionally, a slit aperture can be mounted in front of the camera lens optics to vertically compress interference patterns, reducing the occurrence of pattern overlap (Kobayashi et al. 2000). Further information on the principles of Interferometric droplet sizing can be found in works by Hesselbacher et al. (1991) and Glover et al. (1995).

GSV is commercially available IDS package that incorporates these aspects along with an image processor capable of positioning and sizing droplets imaged using a windowed Fast Fourier Transform (FFT)-based approach (Pan et al. 2006). Assessments of this technique through the use of a mono-disperse droplet generator have shown the method to be reliable, displaying standard deviations of less than 2 µm across a range of known droplet diameters (Davies et al. 2019).

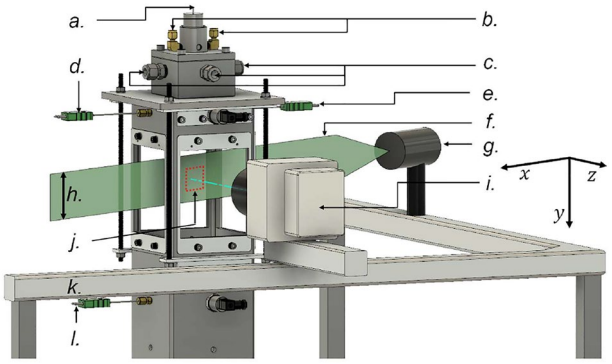

Fig. 3 Sketch of the experimental setup. **a** SONICS atomiser, **b** cooling air inlet, **c** heated air inlet, **d** heated air outlet thermocouple, **e** cooling air thermocouple, **f** laser sheet, **g** LASERPULSE light arm head, **h** laser sheet height (100 mm), **i** phantom VEO 710 camera, **j** measurement volume, **l** downstream thermocouple, **k** 3-axis traverse

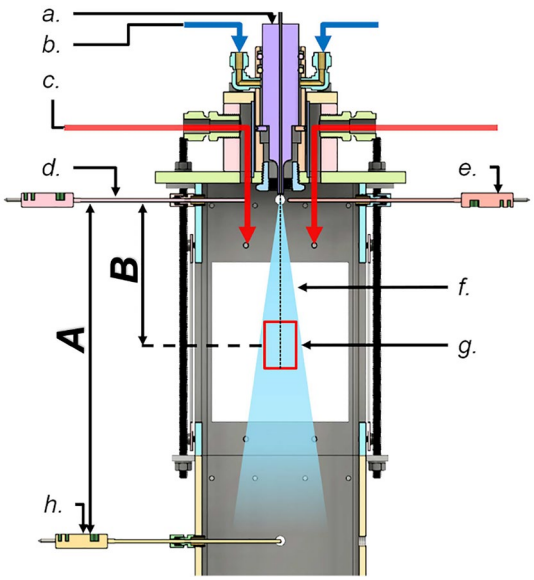

Fig. 4 Sketch of the system used to heat the air and control its temperature through thermocouples. **a** SONICS atomiser, **b** cooling air inlet, **c** heated air flow, **d** heated air outlet thermocouple, **e** cooling air thermocouple, **f** liquid spray, **g** measurement volume region, **h** downstream thermocouple. Lengths A and B being 300 mm and 140 mm, respectively

2 Experimental setup

A custom-made optical rig was designed and employed to measure droplet evaporation rates using planar interferometric droplet tracking under heated flow conditions (See Figs. 2, 3).

The optical rig has a squared cross section with side length of 150 mm and a height of approximately 900 mm. Four 150 mm by 120 mm fused quartz windows allowed optical access, whilst retaining heat within the test rig. An ultrasonic atomiser (Sonics atomiser) was used to produce droplets ranging from approximately 20–150 µm in diameter, whilst a Harvard Apparatus PHD Ultra 70-3006 syringe pump was used to feed the working fluids (both water or methanol) to the atomiser at a rate of 200 ml/hour. The spray was injected into a coaxial heated air flow provided by a process heater connected with a PID controller. Fitted in line, an Alicat-M gas flow meter allowed for precise control of air flow rates (75–200 slpm) and output temperatures (288–550 K). To prevent overheating and damaging of the injection system, the atomiser was cooled down in between tests by an air flow (see Fig. 4). The temperature of both the cooling and heated air flows was monitored using two thermocouples at the corresponding inlets of the spray chamber. In addition, the temperature 300 mm beneath the atomiser nozzle tip was recorded by a thermocouple. For all tests, the heated air flow rate was 100 slpm, and for heated conditions the air temperature at spray chamber inlet was measured at 515 K, whilst the thermocouple located 300 mm downstream measured 475 K. The temperature at the measurement volume (140 mm downstream of the atomiser) was estimated to be 495 K by linear interpolation.

Laser illumination was provided by an EdgeWave IS-series high-speed laser (532 nm, 20 mJ pulse) with a TSI Laserpulse light arm and sheet optic redirecting and reforming the laser beam into a sheet with a thickness of approximately 1.5 mm in the measurement region. A Phantom VEO 710 high-speed camera fitted with a Tokina 100 mm lens and slit aperture mounted at a scattering angle of 60° was used for imaging. For all tests presented in this study, the lens aperture was set to f/5.6 and a 1:1 magnification factor was used at a resolution of 800×1024 pixels, resulting in a field of view measuring ≈ 16 mm in width and 20 mm in height. The laser pulse frequency and camera framerate were set to 7 kHz synchronised using a TSI Laserpulse Synchroniser 610036 and TSI Insight 4G.

To control the positioning of the measurement volume an in-house software-controlled three-axes traverse was developed, allowing for the adjustment along the axial, y, and radial, x, directions of the measurement volume location and camera defocus, $z \csc \theta$ with a displacement resolution of 2.5 µm. This allowed the identification and optimal control measurement location, which is informed by local droplet concentration. On the one hand, a large droplet concentration is desired to increase dataset size and build statistics. On the other hand, it can result in overlap of multiple droplet interference patterns, with a reduced accuracy of the TSI Insight software to detect and size them. The data included in this work were obtained along the spray axis, 140 mm downstream of the nozzle tip, where the average droplet diameter and concentration were 41.4 µm and approximately 300 droplets per cm^3,

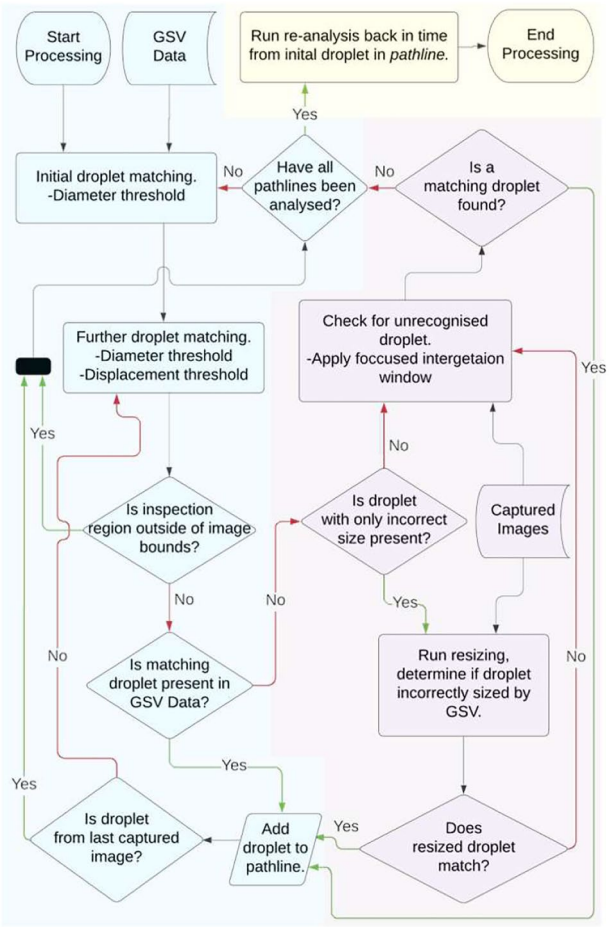

Fig. 5 Flow chart showing the interferometric droplet tracking processor algorithm. (Blue) Droplet tracking from GSV droplet data, (purple) re-analysis of interference patterns incorrectly measured or unrecognised by GSV processor, (yellow) re-analysis of droplets backwards in time

respectively. This droplet concentration level reduced the likelihood of oscillation pattern overlap and allowed the capabilities of the proposed particle tracking methodology to be fully tested. It should be noted that GSV measurements have been shown to be reliable up to concentrations of 3,000 droplets per cm^3 (Pan et al. 2006). The defocus displacement was optimised and set to 20 mm.

3 PIT processor

The developed PIT processor builds upon a pre-existing IDS technique, Global Sizing Velocimetry (GSV) produced by TSI, as a first-pass processor (from raw images the GSV processor outputs the droplet size and 2-D position co-ordinates

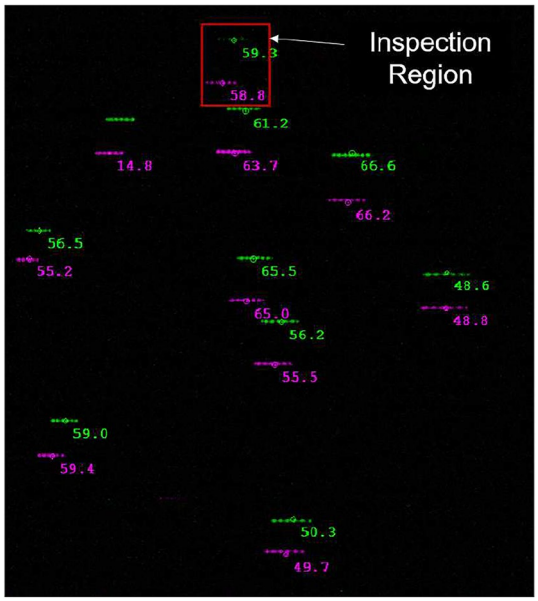

Fig. 6 Two-frame composite GSV image, $Image_1$ (green), $Image_2$ (magenta), with representation of inspection region (red) located about $Drop_1(x, y)$. GSV measured droplet diameters annotated next to respective interference patterns

along with other parameters such as the intensity of interference patterns, but does not provide any tracking details).[1] As shown in the block diagram of Fig. 5, the GSV data are given as an input to the PIT processor algorithm.

The PIT processing algorithm is broken down into three distinct steps, the first of which highlighted in blue within Fig. 5 uses only the data provided by GSV in the tracking of individual droplets. To track a droplet path, it is first necessary to determine its position into two consecutive images. This process is carried out by matching a droplet already detected by GSV in the first image, $Drop_1$, to a droplet detected in the second one, $Drop_2$. The *matching* is made by searching for droplet of similar size to $Drop_1$ in an inspection window, see Fig. 6, built in proximity of its initial location.

The exact dimensions of this inspection window are dependent on the local mean flow velocity and its fluctuation due to turbulence levels; in this study the inspection window had a width of 0.4 mm and a height of 0.6 mm (0.2 mm above the initial position and 0.4 mm below). Matching between $Drop_1$ and different droplets found in the inspection window of the second image is made by finding the $Drop_2$ whose diameter deviates the least from that of $Drop_1$. The level of droplet diameter deviation is tuned with a threshold (e.g. $\pm$ 5%) that takes into account the measurement accuracy and potential evaporation over the time period between two consecutive images.

[1] Pan et al. (2006) describe the specific image processing methods deployed by the GSV processor.

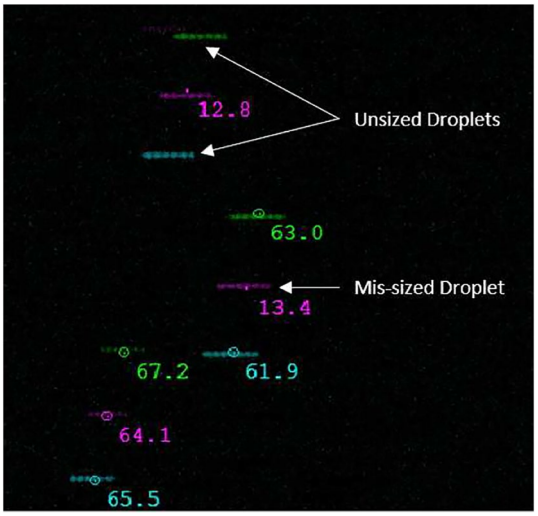

Fig. 7 Example of incorrect measurement/detection of interference patterns. Image_n (Green), Image_{n+1} (Magenta) and Image_{n+2} (cyan)

Having identified an individual droplet in two consecutive frames the droplet position and diameter for the droplet in both Image_1 and Image_2 is recorded, and a droplet *pathline* is created (this being a matrix containing the measured diameter, position, velocity and oscillation pattern intensity history). The following positions assumed by a droplet along its path are found with a similar *droplet matching* process as described above, where the inspection window is moved in proximity of the last droplet position detected. In this case, a second criterion, beside the droplet size deviation, is used to optimise the droplet matching. This accounts for the "projected" droplet displacement, and it is estimated from the velocity of the droplet between its two most recent detections. An allowable deviation from the "projected" position is set, this being based on the turbulent velocity fluctuations within the flow and the uncertainty in droplet position measurement. Should there be more than one droplet meeting the validation criteria, the one with least size deviation from the droplet in the previous frame is selected. It should be noted that the processor also ensures that an individual droplet measurement may only be present within a single *pathline*. The processing procedure is then the same for subsequent frames, with this ending when no valid droplets are discovered or the inspection window reaches the limits of the image region. Once the *pathline* for a droplet is terminated (when a droplet exits the illumination plane or droplet oscillation pattern disappears or is incoherent due to signal attenuation, multiple oscillation patterns overlapping or otherwise), the processor iterates through all droplets in all images that have not been already included within a *pathline*.

Though an effective measurement technique, GSV often can either incorrectly measure droplet sizes or not detect

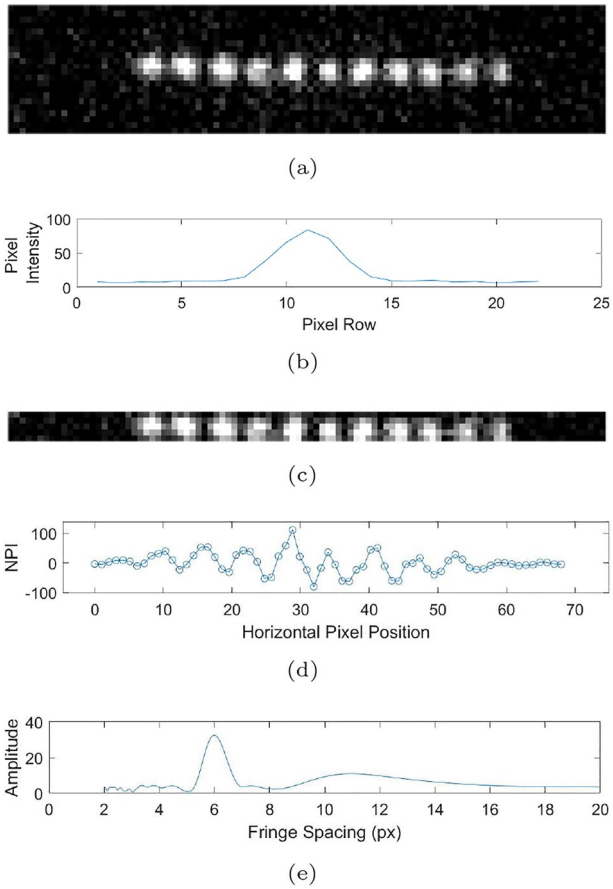

Fig. 8 **a** Focused inspection window for interference pattern re-analysis, **b** mean row pixel intensity vertically across the inspection region, **c** focused inspection region slice located about interference pattern vertical centre, **d** Mean Normalised Pixel Intensity (NPI) profile of Focused inspection region with Hamming taper, **e** FFT and spatial period identification (Fringe Spacing)

all interference patterns present in an image, as shown in Fig. 7, as is common among many IDS systems. Typically, only 50–75% of the interference patterns are measured, with the remaining patterns not passing signal-to-noise ratio threshold, or not being detected at all. In addition, a number of oscillation patterns are incorrectly measured, typically significantly underestimated, preventing them from being included within a droplet pathline (Davies et al. 2019). These inconsistencies in droplet detection and sizing have an inevitable impact on the droplet pathline detection. To provide a more complete dataset, the PIT processor developed in this work re-analyses areas within an image where a droplet of a given size is expected to be according to its previous path. This extra analysis aims to correct mis-sized droplets by GSV or measure interference patterns that had been originally discarded/undetected by GSV. Thus, further image processing is required, which is highlighted in purple in the block diagram of Fig. 5.

For both mis-sized and undetected droplets, the PIT processor applies a focused inspection window about the predicted interference pattern position, as shown in Fig. 8a, determined by extrapolation. The vertical position of the interference pattern is then determined by analysing the mean pixel intensity of each row of the focused inspection window. The pixel rows containing the interference pattern are then vertically compressed by taking the mean of each column. The horizontal centre point of interference pattern within the 1-D mean intensity vector is determined through the use of a continuous wavelet transform as performed by Hardalupas et al. (2010, 2014). A taper is applied to this intensity vector before a Fast Fourier Transform (FFT) is used to determine the interference pattern spatial period, as shown in Fig. 8d.

As documented by Pan et al. (2006), the droplet diameter can then be determined through the use of Eqs. 1 and 2. At a 60° scattering angle, the fringe spacing is very marginally affected by the refractive index of the liquid in use, and as such, a generalised value of $X = 1.129$ has been used (Pan et al. 2006; Calabria and Massoli 2000). The fringe angular spacing, $\Delta\zeta$, can be expressed in terms of the lens magnification after defocus (M), pixel size (δ), defocussing distance (Δz) and fringe spacing in pixels (n):

$$\Delta\zeta = \frac{M \cdot n \cdot \delta}{\Delta z} \tag{2}$$

Based on this assumption, the droplet size can be calculated from the interference pattern fringe spacing as obtained from the FFT. Comparisons between diameter measurements of the same droplets by PIT and GSV show good agreement with a mean difference of less than 0.5 µm and a standard deviation of approximately 0.75 µm, which is within the expected measurement uncertainty of the system. The additional processing element developed in this work increases substantially the number of detection of a droplet along its path and therefore captures to a higher degree a droplet spatio-temporal evolution and associated evaporation processes.

To further maximise the number of times, a single droplet was measured over time; image datasets were also subject to a backward analysis, where the same process as described above was implemented starting from droplets present in the last image and extrapolating their previous position moving backward in time (yellow block in Fig. 5).

4 Non-evaporating spray

To assess the performance of the PIT processor and outline the potential errors present within the droplet history and position measurements, a sequence of 771 images were captured, with water being used as the atomising liquid.

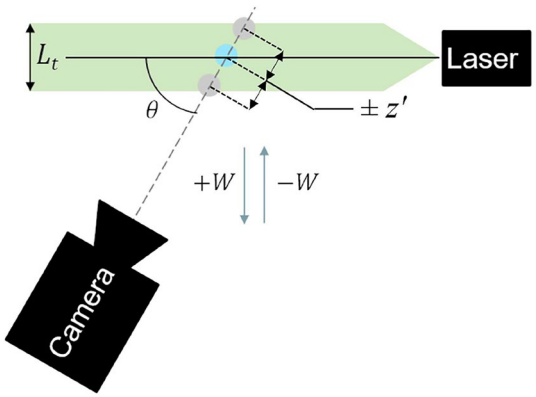

Fig. 9 Droplet camera orientation resulting in droplet defocus uncertainty. Blue droplet representing the processor assumed defocus and grey droplets representing potential extreme defocus positions

This spray produced a profile of droplet diameters with a mean droplet diameter of 41.4 µm that can be approximately described as following a lognormal distribution (μ= 3.6, σ= 0.4) and concentrations at the measurement volume of up to approximately 300 drops/cm^3. The mean radial and axial droplet velocities were measured by PIT to be 0.06 m/s and 0.67 m/s, respectively. These tests were performed at atmospheric pressure and room temperature. Under these conditions, droplet diameter reductions due to evaporation are likely negligible,[2] thus any trends in temporal droplet size evolution identified in the dataset is likely due to measurement error.

The greatest source of uncertainty in the instantaneous measurement of droplet size is due to the thickness of the laser sheet and the transit time and path across the measurement volume taken by the droplet (i.e. out-of-plane velocity, W). All these variables directly affect the droplet defocus, which is assumed by the processor to be constant at a particular point in an image (i.e. perfect 2D plane with zero thickness). As shown in Eqs. 1 and 2, a droplet measured size is proportional to the actual defocus, and therefore, any uncertainty in defocus directly affects the measured diameter. From geometrical considerations (see the sketch in Fig. 9), the maximum defocus deviation, z', from the prescribed 2D constant value, can be estimated from Eq. 3,

$$z' = \pm\frac{L_t}{2} \cdot \sec\theta \tag{3}$$

where L_t is the laser sheet thickness, $\theta = 60°$ for GSV.

In time-resolved droplet sizing, the droplet defocus uncertainty can result in a non-evaporating droplet apparently

[2] Estimations made using a droplet evaporation model mentioned in greater detail in subsequent sections is <0.2 µm over 10 ms for a 20 µm diameter droplet.

Table 1 Calculated proportional droplet surface area change due to out-of-plane velocity at image centreline

Effective laser sheet thickness (mm)	$E\,[+W]\,(\%)$	$E\,[-W]\,(\%)$
0.25	− 2.47	2.53
0.50	− 4.88	5.13
1.00	− 9.52	10.52
2.00	− 18.14	22.16

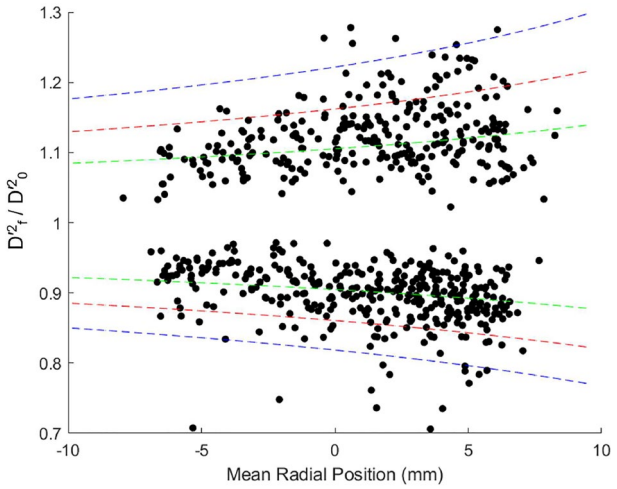

Fig. 10 Final-to-initial droplet surface area ratio for non-evaporating spray, markers showing experimental data. Dashed lines showing expected error due to defocus variation with laser thickness transit for sheet of thickness: 2 mm (blue), 1.5 mm (red), 1.0 mm (green)

increasing or decreasing in size, depending on the droplet out-of-plane direction. In the case of a droplet moving towards the camera, $+W$, the actual defocus will decrease as it travels through the laser sheet. Conversely, when moving away from the camera $(-W)$ the actual defocus increases. The effect of the droplet out-of-plane motion and defocus impact on droplet size can be determined using Eqs. 1 and 2, where it is apparent the error in proportional droplet surface change from initial droplet diameter (D_0) to final droplet diameter (D_f) due to change in actual defocus, E; Eq. 4. E is only a function of the radial position of the droplet within the image, droplet out-of-plane direction $(\pm W)$ and the laser sheet thickness, and independent of droplet diameter. Table 1 shows the estimated error in final-to-initial droplet surface area ratio at the image centreline for relevant laser sheet thicknesses. (Note: these values may change for different optical setups).

$$E = \frac{D_f^2}{D_0^2} \tag{4}$$

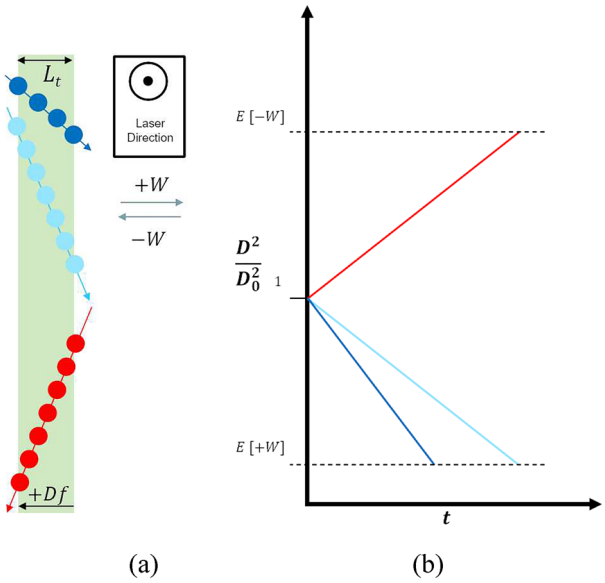

Fig. 11 **a** Diagram showing three droplets (dark blue, light blue and red) transiting laser sheet thickness due to their out-of-plane velocity, W, where $+Df$ shows direction of increasing defocus, **b** proportion droplet surafce area versus time for the three droplets

Figure 10 shows the variation in the measured final-to-initial droplet external surface area ratio, against their corresponding mean radial positions for water droplets at a temperature of 300 K. The dashed lines indicate the theoretical maximum potential error magnitude, E, due to defocus for three possible laser thicknesses, L_t=1, 1.5 and 2 mm. The experiments were run with water, and taking into account the temperature, the size of the image window and measurement timescale, no significant evaporation is expected for these conditions (i.e. no variation in D_f/D_0). However, according to Fig. 10 the variation in measured droplet surface from its initial value can vary between 5 and 20%. It is clear that the apparent increase or decrease in final-to-initial external surface area ratio closely follows the variation in the theoretical error due to droplet defocus with radial distance.

Figure 11a, b illustrates how the out-of-plane velocity, W, magnitude and direction affect the droplet measurement as droplet transit through the laser sheet. In the case of the two droplets with a decreasing defocus, $+W$, shown as dark blue and light blue in Fig. 11a, they will both experience the same level of defocus, resulting in an erroneous proportional droplet diameter change. However, the darker droplet will go through this process in a shorter time and therefore exhibits an erroneous higher rate of droplet surface area variation as line gradients depict in Fig. 11b.

It is possible to correct for the measurement error due to the variation in the droplet defocus across the measurement volume when the out-of-plane droplet direction is known. In

non-evaporating conditions, droplet out-of-plane direction can be determined by observing whether measured droplet diameter increases or decreases with time.[3] This is well elucidated in Eq. 5:

$$\frac{D'^2}{D_0'^2} = \frac{D^{\cancel{2}^{1}}}{\cancel{D_0^2}} \pm \frac{E}{t_{total}} \cdot t \tag{5}$$

where D_0' is the measured droplet diameter at $t = 0$, D_0 is the actual initial droplet diameter at $t = 0$, D and D' are the actual and measured droplet sizes at t, where $0 < t < t_{\text{total}}$, t_{total} being the time taken for the droplet to completely transit the laser sheet thickness. As no appreciable droplet diameter change is likely in the experimental conditions described in this section, the actual droplet surface area should not vary over time. Rearranging Equation 5 into 6, it is clear that the error associated with defocus variation due to out-of-plane motion will manifest as a linear increase or decrease in droplet diameter with time.[4]

$$D'^2 = D_0'^2 \pm \frac{E \cdot D_0'^2}{t_{\text{total}}} \cdot t \tag{6}$$

As E, D_0', t_{total} and t are known values it is possible to remove this linear error through subtraction. It should be noted that this error subtraction is applicable only to droplets, which could be tracked across the entire control volume thickness, between the front and back faces of the laser sheet. This process can be monitored by checking the intensity of the light scattered signal of the same droplet at different instances, as this will display an increase (decrease) as the droplet moves towards (away from) the mid-section of the laser sheet thickness (i.e. the laser sheet intensity has a gaussian-like distribution across its thickness).

[3] In evaporating conditions, it is not sufficient to determine the out-of-plane direction through observing the droplet diameter change. The authors of this paper propose that the change in interference pattern width could be used to determine the direction of droplet out-of-plane motion, as is explained by Damaschke et al. (2002, 2005) and Kawaguchi et al. (2010). This would allow for the removal of defocus error in evaporating sprays. This idea was tested as part of this study, though the relatively large pixel size (20 μm) for the optics selected did not allow to spatially resolve the variation in time of the interference pattern width as droplets cross the measurement volume. Similar problematics were also reported by Sugimoto et al. (2006) when trying to determine the out-of-plane velocity from the rate of change of interference pattern width. They then reported that a stereoscopic IDS method would offer a more viable solution for defining droplet out-of-plane velocity.

[4] Though not within the scope of this study, it stands to reason that the gradient associated with erroneous droplet diameter increase is proportional to the droplet out-of-plane velocity; thus, analysis of the apparent diameter change could be used to determine droplet 3-component velocity in non-evaporating conditions.

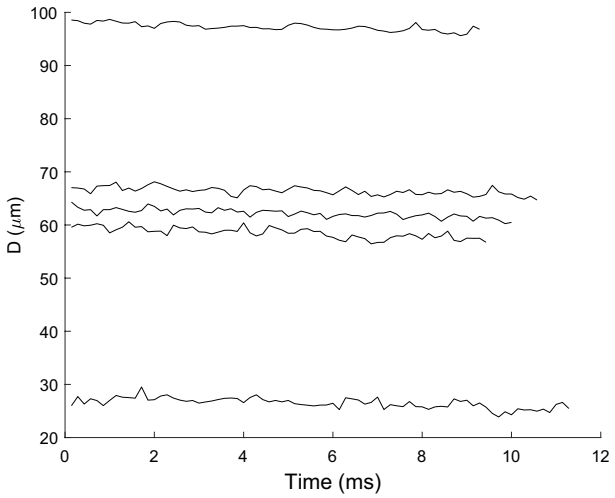

Fig. 12 Examples of droplet diameter time evolution

Figure 12 shows examples of corrected droplet diameter variation with time for five water droplets at 18°C, which fully transited through the laser sheet thickness. After correction, droplet diameter measurements display a similar random error, irrespective of their diameter, which varies within a range of ± 2 μm, as shown in Fig. 12. This error is likely due to signal noise, aliasing, attenuation and the multiple scattering of light, which all affect the interference pattern intensity.

These aberrations of the interference patterns can be caused by the overlap of two droplets fringes or by droplets sitting out of the illumination plane further scattering the refracted/reflected light from a droplet, both resulting in inconsistencies in the droplet size measurement. This measurement uncertainty is common to all standard IDS measurement techniques, including both GSV (Davies et al. 2019) and the current PIT method discussed in this work. Direct comparison of droplets measured either with GSV or PIT indicated that the two methods produce consistent measurements with similar uncertainty levels. The uncertainty in measurement can be improved by increasing the spatial resolution of the camera and optics.

The proposed tracking method is not only capable of fully resolving droplet pathlines and therefore assesses measurement uncertainty, but can increase significantly the number of valid interference pattern measurements in comparison to standard GSV processor. As an example from a sample sequence of 771 images, the standard GSV processor detected and measured 31,510 interference patterns of which 23,541 passed the PIT validation criteria and were used in the tracking of droplets. An additional 11,100 interference patterns were detected through the PIT processor that had been either miss-sized or undetected by the standard GSV processor. These 11,100 interference patterns had their

diameter and position determined and then included into a droplet pathline as part of the tracking data. This equates to a 47.3% increase in valid interference patterns being included in droplet tracking through the use of the PIT processor. From this set of images, a single droplet was tracked over a sequence of 182 images (26 ms) with 118 of the 182 interference pattern measurements being made by the PIT processor.

5 Evaporating spray

Having identified and analysed different sources of measurement error present in a non-evaporating spray, the PIT processor was then applied to a methanol spray in a heated coaxial air flow. To select the experimental conditions, a series of preliminary tests were carried out. The measurement window position is approximately 155 mm from the heated air outlet, y_m, (see Fig. 4) and as such should be located within the hydrodynamic entrance region ($\frac{y_m}{R_H} \approx 1$, where R_H is the hydraulic radius). A hot wire anemometer, RS PRO DT-8880 was used to determine the local air velocity magnitude in proximity of the measurement region. The recorded mean air velocity at the measurement position was 0.63 m/s. This is in agreement with the droplet axial velocities obtained using PIT, which are normally distributed about a mean of 0.66 m/s with a standard deviation for the entire volume of 0.25 m/s. These levels of local velocity fluctuations and turbulence are consistent with the unsteady nature of the flow present within the inner mixing region of the expanded annular coaxial flow (Ko and Chan 1978, 1979).

The rates of droplet evaporation obtained from the proposed PIT method under realistic evaporating conditions are compared against those derived from a methanol-adapted droplet evaporation model (Davies 2022). This is an iterative model developed by Lefebvre and McDonell (2017), which accounts for the change in droplet diameter, D, and droplet surface temperature, T_s, over a short time period, dt. In addition to calculating the steady state evaporation rate, k, commonly described by the D^2 *law* of Eq. 7, this model also accounts for the initial "heating up period" where the droplet surface temperature increases when subject to high ambient temperatures. The evaporation model was adapted to methanol by using fuel-specific curves to account for the variation with temperature of the vapour pressure (Arce et al. 1997), thermal conductivity (Touloukian et al. 1970), vapour and liquid specific heat (Strömsöe et al. 1970; Khasanshin and Zykova 1989), latent heat (Majer and Svoboda 1986) and density (Vogel and Weiss 1982).

$$D_0^2 - D^2 = \kappa t \tag{7}$$

For a flow with an ambient air temperature of 495±10 K, the model predicts that all droplets of applicable diameters, ≤ 250 µm, would have reached a stable surface temperature for the given air and droplet velocity conditions. As such, according to the model, the rate of surface area reduction, κ, should be constant for all droplets within the measurement volume, with a predicted steady state evaporation constant of 43.3 ± 2.5 µm^2/ms.

For this study, a total of 28 repeat tests were performed with 770 images captured in each test (21,560 images in total). From these images, a total of 24,343 individual droplets were identified and tracked. The measured droplet mean diameter for the total dataset was 62.36 µm.

To accurately assess the change in droplet diameter in evaporating conditions, the contribution of the error due to droplet defocus on the rate of reduction in the final to initial surface ratio must be considered. According to Eq. 5 and its time derivative, Eq. 8, the accuracy of the measurement for a given laser sheet thickness increases when the actual rate of droplet evaporation, κ, is significantly larger than the error due to the rate of change of defocus, $\frac{E}{t_{\text{total}}}$. This condition can be achieved when the total residence time of a droplet within the measurement volume, t_{total}, is large. In essence, the capability of the PIT technique to accurately determine the droplet diameter reduction due to evaporation is limited by the actual evaporation rate of the droplets in comparison with the defocus error, E, and the duration for which they reside within the measurement volume.

$$\begin{aligned} \frac{\mathrm{d}}{\mathrm{d}t}\left(\frac{D'^2}{D_0'^2}\right) &= \frac{\mathrm{d}}{\mathrm{d}t}\left(\frac{D^2}{D_0^2}\right) \pm \frac{E}{t_{\text{total}}} \\ \frac{\mathrm{d}}{\mathrm{d}t}\left(\frac{D^2}{D_0^2}\right) &= \frac{-\kappa}{D_0^2} \gg \frac{E}{t_{\text{total}}} \end{aligned} \tag{8}$$

In this study, the ratio, ψ, Eq. 9 between the measured rate of change of proportional droplet surface area and the rate of change due to the defocus error, is considered to assess the measurement accuracy.

$$\psi = \frac{\frac{\mathrm{d}}{\mathrm{d}t}\left(\frac{D'^2}{D_0'^2}\right)}{\frac{E}{t_{\text{total}}}} \tag{9}$$

A comparison between the model predicted droplet surface area reduction rate and that measured by PIT is shown in Fig. 13. The data points are colour coded based on the value of ψ, which takes into account their residence time in the laser sheet. As mentioned above, larger values of ψ correspond to a lower impact of the defocus error. These data points (green and blue, $\psi > 1$) are scattered around the 45°

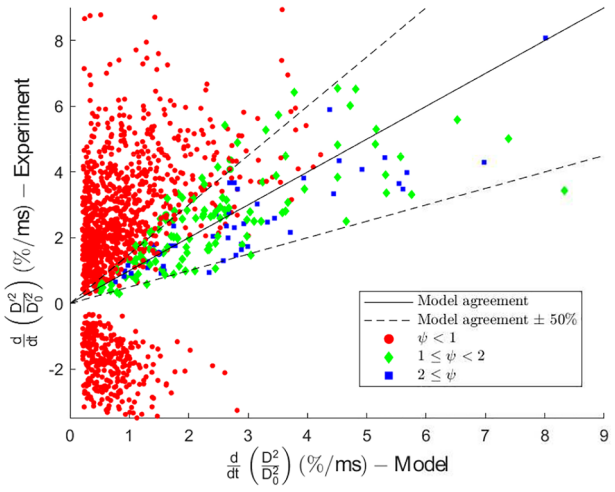

Fig. 13 Model experiment comparison of proportional droplet surface area reduction rate, $\frac{d}{dt}\left(\frac{D^2}{D_0^2}\right)$. Marker colour showing ratio of proportional droplet surface area reduction rate to expected due to rate of change of defocus, ψ, (blue—square) $\psi \geq 2$, (green—diamond) $1 \leq \psi < 2$, (red—circle) $\psi < 1$. Solid central line showing perfect agreement between model and experiment, dashed lines showing a deviation from the model prediction by ± 50%

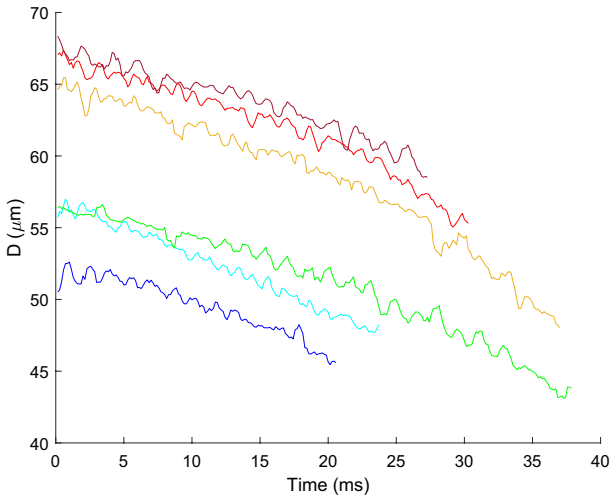

Fig. 14 Droplet diameter change with time for six droplets transiting the measurement volume height

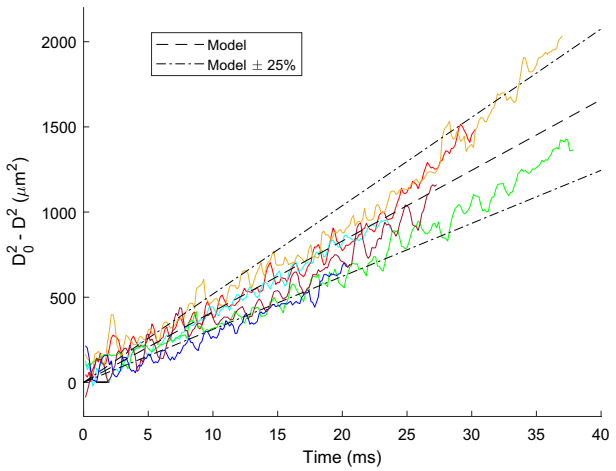

Fig. 15 Droplet surface change with time due to droplet evaporation for droplets with residence time greater than 20 ms. Reference lines in representing the model predicted κ_{Model} (Solid) ± 25% (Dashed)

line indicating a reasonably good agreement between the experiments and the model. However, when ψ <1, several data points exhibit variation well outside of the reference lines (±50%). In particular, points with negative reduction rates are indicative of an increase in droplet diameter which is completely nonphysical and are mainly due to the droplets degree of defocus increasing in time as they cross the control volume. It is worth mentioning that none of the droplets associated with a lower percentage error, ψ >1, are characterised by a negative and nonphysical surface reduction rates. Agreement between the model and measurements does not seem to increase significantly with increasing value of ψ, though it should be noted that the sample size of droplets with values of $\psi > 1$ is very low. From the 24,343 individual droplets tracked by PIT, only 166 have measurement to error ratios greater than one, 0.68% of the total dataset.

For the 166 droplets with $\psi > 1$, the mean and standard deviation of the evaporation rate constant, κ, were 41.74 μm²/ms and 15.28 μm²/ms, respectively, with data points following a normal distribution. Despite the large standard deviation due to the errors outlined previously, the mean evaporation constant as measured by PIT compared relatively well with the value predicted by the model, 43.3 ± 2.5 μm²/ms.

The data were further analysed to identify those droplets with small out-of-plane velocity component. These droplets did not fully traverse the laser sheet thickness, but entered at the top of the measurement volume, traversed the full vertical height of the image (≈20 mm), and then left at the bottom of the measurement volume. As the magnitude of out-of-plane velocity for these droplets is small, their measured droplet diameter is subject to minimal error due to change in defocus. As would be expected, droplets having sufficiently small out-of-plane velocities were seen to predominantly be droplets with higher axial momentum. The combination of larger droplet diameters, most of which were in excess of 150 μm, and low measurement volume residence times, meant many of the droplets fully transiting the measurement volume height did not show any significant size variation. From the current experiments only six droplets fitting the criteria mentioned above were observed. The diameter time evolution of these droplet is shown in Fig. 14. For all of them, a clear decay in droplet diameter with time is

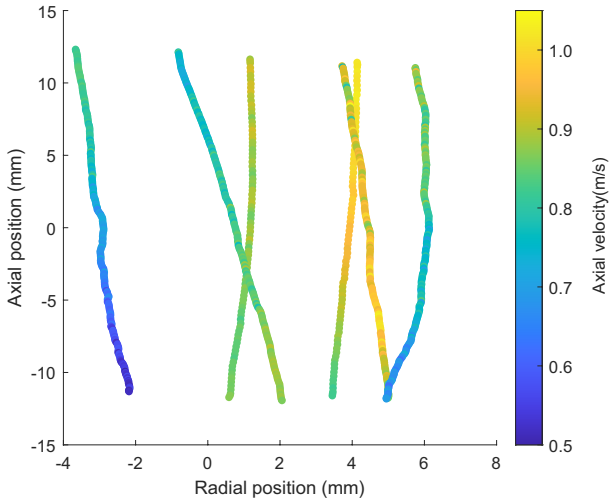

Fig. 16 Visualisation of the pathlines for the six tracked droplets with colour indicating the instantaneous axial velocity

seen, much greater in magnitude than the apparent random variation due to noise.

Figure 15 shows the change between the initial and instantaneous droplet surface area over time. Assuming the droplets are in steady-state evaporation, the rate of change in droplet surface area should be constant, in accordance with the D^2 law. The data shown in Fig. 15 are in reasonable agreement with this model, as the rate of droplet surface decrease is characterised by a nearly linear variation with time. The evaporation rate constant of these droplets was found to agree within a ±25% margin with that derived from the prediction model, a considerable reduction from the ±50% deviation in results shown in Fig. 13. This clearly indicates that as the expected error due to the droplet defocus is reduced, the agreement between measurements and model improves.

The variation in evaporation rates displayed in Fig. 15 may not be only a result of the described measurement error . A proportion of the variation might be related to air flow temperature fluctuation and the presence of convection (not accounted for in the simple model). As previously described, a turbulent flow region is expected within the measurement volume and has been confirmed by the variation in droplet velocities observed through PIT measurements. Indeed, the recorded velocities of the six tracked droplet reported in Fig. 16 show a considerable difference from the mean flow velocity (0.6 m/s). In such a flow regime, the slip velocity between the gas and liquid phases could fluctuate and therefore have an impact on the convection coefficient. To estimate the extent to which slip velocity and convection effect the evaporation rate, an additional factor based on droplet Reynolds and Prandtl numbers (Lefebvre and McDonell 2017) was incoorperated into the evaporation model. For a range of slip velocities, 0.01-0.3 m/s, the increase in predicted evaporation rate was observed to be between 5 and 30%, respectively. This increase is consistent to the variation in evaporation rates observed in Fig. 15. The air flow temperature fluctuation observed in this study could introduce an additional uncertainty in evaporation rate, the magnitude of which is estimated to be approximately 6%. In order to fully understand the influence of flow parameters on droplet evaporation rate, detailed measurements of individual droplet velocity and temperature histories would be required.

6 Conclusion

In this work, a Lagrangian Planar Interferometric Tracking (PIT) processor based on high-speed planar interferometric imaging has been developed. Initially using the TSI Global Sizing Velocimetry, GSV, droplet diameters and positions within the image window were determined. From these initial data, individual droplets are identified and tracked over multiple frames through a combination of validation factors. In the event that the GSV processor incorrectly analyses an interference pattern, the PIT processor uses a targeted Fast Fourier Transform to re-analsyse image regions, thus allowing to further track individual droplets. The PIT method allowed to increase the number of valid droplet measurements by 47.3% as compared to those identified by the GSV processor.

From observing droplet diameter change over time, an inherent measurement uncertainty within all planar interferometric droplet sizing (IDS) techniques became apparent. Uncertainty in the actual droplet defocus, dependant on droplet out-of-plane velocity and laser sheet thickness, resulted in considerable diameter measurement uncertainty. This uncertainty increases with laser sheet thickness, though even for relatively thin sheets the effects are noticeable, and for instance, the estimated diameter measurement uncertainty when using a 0.5-mm-thick laser sheet is ±5%. With the use of PIT, this measurement uncertainty is seen to manifest as an erroneous increase or decrease in droplet diameter over time. This aspect was tested on experimental data obtained in non-evaporating conditions, and it was found that the measured droplet diameter showed a variation in time in agreement with that predicted by the defocus error source identified in this work.

The removal or reduction in error associated with the change in defocus distance can be resolved simply by determining the direction of droplet out-of-plane travel which could be performed using three potential methods:

- In non-evaporating conditions, droplet out-of-plane direction can be determined by the apparent increase or decrease in a tracked droplets diameter, this being

shown in this paper to be effective. This method also potentially allowing for the determination of droplet out-of-plane velocity, though this was not tested as part of this study.
- In both non-evaporating and evaporating conditions, the change in oscillation pattern length may be used to determine the out-of-plane direction, though this method is sensitive to optical spatial resolution and was not found to be practical given the hardware used in this study.
- In both non-evaporating and evaporating conditions, a stereoscopic PIT method could be used to determine droplet out-of-plane velocity/direction.

PIT was seen to be capable of tracking methanol droplets transiting a $16 \times 20 \times 1.5$ mm measurement volume, in ambient air temperatures of 495 K. On initial inspection of the measured evaporation rates, considerable variation is seen, due to the outlined error resulting from the droplet out-of-plane velocity.

By analysing droplet data effected to a lesser degree by the outlined error, the PIT system was seen to detect the evaporation rates of heated methanol droplets with good agreement to a model modified for methanol. PIT measured droplets were seen to have evaporation constants within $\pm 25\%$ of the model prediction. A significant proportion of observed difference in measurement and model outcomes could be attributed to complex droplet–flow interactions not accounted for by the basic model.

Acknowledgements The authors would like to acknowledge the valuable input from both Dr. Suresh Sadasivuni and Dr. Daniel Lörstad of Siemens Energy.

Author contributions Mr. HD took part in concept development, experimentation, data analysis and manuscript writing. Dr. MT involved in design and experimentation supervision, manuscript writing. Dr. AD took part in data reduction supervision and manuscript writing. Mr. NP involved in data analysis (evaporation model). Prof. RB took part in project lead, concept development, secured funding, supervision, manuscript writing.

Funding The authors gratefully acknowledge support from UKRI Future Leaders Fellowship (MR/T019735/1) and UCL Mechanical Engineering (studentship for Mr. Hywel Davies) towards this work.

Declarations

Conflict of interest The authors have no competing interests to declare that are relevant to the content of this article.

References

Abramzon B, Sirignano WA (1989) Droplet vaporization model for spray combustion calculations. Int J Heat Mass Transf 32(9):1605–1618

Arce A, Blanco A, Soto A et al (1997) Phase equilibria of water+ methanol+ hexyl acetate mixtures. Fluid Phase Equilib 128(1–2):261–270

Bachalo W, Houser M (1984) Phase/doppler spray analyzer for simultaneous measurements of drop size and velocity distributions. Opt Eng 23(5):235–583

Balachandran R, Chakravarthy S, Sujith R (2008) Characterization of an acoustically self-excited combustor for spray evaporation. J Propul Power 24(6):1382–1389

Bautista-Capetillo C, Robles O, Salinas H et al (2014) A particle tracking velocimetry technique for drop characterization in agricultural sprinklers. Irrig Sci 32(6):437–447

Calabria R, Massoli P (2000) Experimental study of droplets in evaporating regime by 2d scattering analysis. In: 10th International symposium on applications of laser techniques

Chauveau C, Birouk M, Halter F et al (2019) An analysis of the droplet support fiber effect on the evaporation process. Int J Heat Mass Transf 128:885–891

Chen Y, Guildenbecher DR (2017) Quantitative, bias-corrected measurements of droplet position, size and velocity with digital in-line holography. In: ILASS Americas 29th annual conference on liquid atomization and spray systems

Chiu H, Kim H, Croke E (1982) Internal group combustion of liquid droplets. In: Symposium (international) on combustion. Elsevier, pp 971–980

Cotabarren IM, Bertín D, Razuc M et al (2018) Modelling of the spray drying process for particle design. Chem Eng Res Des 132:1091–1104

Damaschke N, Nobach H, Tropea C (2002) Optical limits of particle concentration for multi-dimensional particle sizing techniques in fluid mechanics. Exp Fluids 32(2):143–152

Damaschke N, Nobach H, Nonn TI et al (2005) Multi-dimensional particle sizing techniques. Exp Fluids 39(2):336–350

Davies H (2022) Characterisation of evaporating and non-evaporating sprays using planar laser diagnostics and Lagrangian tracking. PhD thesis, University College London, unpublished thesis

Davies H, Talibi M, Hyde M, et al (2019) Investigating ethanol-gasoline spray characteristics using an interferometric drop sizing technique. In: Turbo expo: power for land, sea, and air, American Society of Mechanical Engineers, p V006T05A023

Falgout Z, Chen Y, Guildenbecher DR (2019) Improving the spatial dynamic range of digital inline particle holography. Appl Opt 58(5):A65–A73

Glover A, Skippon S, Boyle R (1995) Interferometric laser imaging for droplet sizing: a method for droplet-size measurement in sparse spray systems. Appl Opt 34(36):8409–8421

Guildenbecher DR, Cooper MA, Sojka PE (2016) High-speed (20 khz) digital in-line holography for transient particle tracking and sizing in multiphase flows. Appl Opt 55(11):2892–2903

Hardalupas Y, Sahu S, Taylor AM et al (2010) Simultaneous planar measurement of droplet velocity and size with gas phase velocities in a spray by combined ilids and piv techniques. Exp Fluids 49(2):417–434

Hardalupas Y, Taylor A, Zarogoulidis K (2014) Detection and evaluation of droplet and bubble fringe patterns in images of planar interferometric measurement techniques using the wavelet transform. In: International conference on optical particle characterization (OPC 2014), SPIE, pp 65–70

Hesselbacher KH, Anders K, Frohn A (1991) Experimental investigation of gaussian beam effects on the accuracy of a droplet sizing method. Appl Opt 30(33):4930–4935

Hubbard G, Denny V, Mills A (1975) Droplet evaporation: effects of transients and variable properties. Int J Heat Mass Transf 18(9):1003–1008

Kawaguchi T, Satoh I, Saito T (2010) Dynamic ilids measurement by means of high-speed nd: Ylf laser. In: Proceedings 23rd annual conference on liquid atomization and spray systems, ILASS-Europe, 2010

Khasanshin T, Zykova T (1989) Specific heat of saturated monatomic alcohols. J Eng Phys 56(6):698–700

Ko N, Chan W (1978) Similarity in the initial region of annular jets: three configurations. J Fluid Mech 84(4):641–656

Ko N, Chan W (1979) The inner regions of annular jets. J Fluid Mech 93(3):549–584

Kobayashi T, Kawaguchi T, Maeda M (2000) Measurement of spray flow by an improved interferometric laser imaging droplet sizing (ilids) system. In: 10th international symposium on applications of laser techniques

Labowsky M (1976) The effects of nearest neighbor interactions on the evaporation rate of cloud particles. Chem Eng Sci 31(9):803–813

Lefebvre AH, McDonell VG (2017) Atomization and sprays. CRC Press

Lieber C, Koch R, Bauer HJ (2019) Microscopic imaging spray diagnostics under high temperature conditions: application to urea-water sprays. Appl Sci 9(20):4403

Majer V, Svoboda V (1986) Enthalpies of vaporization of organic compounds: a critical review and data compilation

Pan G, Shakal J, Lai W, et al (2006) Spray features investigated by gsv: a new planar laser technique. In: Tenth international conference on liquid atomization and spray systems (ICLASS), Kyoto, Japan, Aug

Parant G, Zimmer L, Renaud A, et al (2021) Adaptation of the ptv method for droplets evaporating in vicinity of a flame

Sahu S, Hardalupas Y, Taylor A (2018) Interaction of droplet dispersion and evaporation in a polydispersed spray. J Fluid Mech 846:37–81

Sazhin SS (2006) Advanced models of fuel droplet heating and evaporation. Prog Energy Combust Sci 32(2):162–214

Sommerfeld M (1998) Analysis of isothermal and evaporating turbulent sprays by phase-doppler anemometry and numerical calculations. Int J Heat Fluid Flow 19(2):173–186

Strizhak P, Volkov R, Castanet G et al (2018) Heating and evaporation of suspended water droplets: experimental studies and modelling. Int J Heat Mass Transf 127:92–106

Strömsöe E, Rönne H, Lydersen A (1970) Heat capacity of alcohol vapors at atmospheric pressure. J Chem Eng Data 15(286–290):18

Sugimoto D, Zarogoulidis K, Kawaguchi T, et al (2006) Extension of the compressed interferometric particle sizing technique for three component velocity measurements. In: 13th international symposium on applications of laser techniques to fluid mechanics Lisbon, Portugal, pp 26–29

Sujith R, Waldherr G, Jagoda J et al (2000) Experimental investigation of the evaporation of droplets in axial acoustic fields. J Propul Power 16(2):278–285

Touloukian Y, Liley P, Saxena S (1970) Thermal conductivity: Nonmetallic liquids and gases, ifi

Vogel H, Weiss A (1982) Transport properties of liquids. iv. Self-diffusion, viscosity, and density of irregular liquid mixtures: Crown ether/alcohol. Berichte der Bunsengesellschaft für physikalische Chemie 86(7):615–620

Yarin A, Brenn G, Kastner O et al (1999) Evaporation of acoustically levitated droplets. J Fluid Mech 399:151–204